IEEE Photonics Journal
An IEEE Photonics Society Publication

Open Access

Intersublevel Photoabsorption and Photoelectric Processes in ZnO Quantum Dot Embedded in HfO_2 and AlN Matrices

Volume 6, Number 5, October 2014

D. Maikhuri
S. P. Purohit
K. C. Mathur

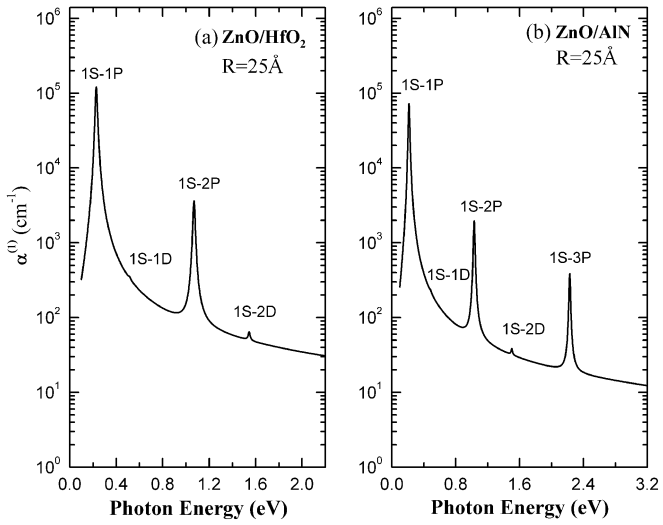

DOI: 10.1109/JPHOT.2014.2317677
1943-0655

Intersublevel Photoabsorption and Photoelectric Processes in ZnO Quantum Dot Embedded in HfO_2 and AlN Matrices

D. Maikhuri, S. P. Purohit,[1] and K. C. Mathur[1]

Department of Physics and Materials Science and Engineering, Jaypee Institute of Information Technology, Noida 201 307, India

DOI: 10.1109/JPHOT.2014.2317677

Manuscript received February 13, 2014; revised March 31, 2014; accepted April 4, 2014. Date of publication April 15, 2014; date of current version September 19, 2014. Corresponding author: S. P. Purohit (e-mail: sppurohitjiit@gmail.com).

Abstract: In this paper, we investigate the linear and nonlinear photoabsorption processes in the conduction-band-confined levels of a singly charged ZnO quantum dot (QD) surrounded by HfO_2 and AlN matrices. We also investigate the photoelectric process in which the conduction band electron ejects from the dot to the vacuum. We use the effective mass approximation with a finite barrier height at the dot–matrix interface. We consider the self-energy of the electron in the dot and the local field effect. The electromagnetic interaction of the incident radiation with the electron in the dot is considered in the electric dipole plus quadrupole approximation. Results for the photoabsorption coefficient and the photoelectric process are presented for different dot sizes and different intensities of incident radiation. It is found that the inclusion of the quadrupole effect reveals new photoabsorption peaks in the absorption spectra. Both the photoabsorption and photoelectric processes significantly depend on the dot size and the surrounding matrix. The change in the intensity of the incident radiation significantly influences the nonlinear photoabsorption. The photoabsorption coefficient and the photoelectric cross sections are found to be relatively higher for the ZnO QD embedded in the high-dielectric constant matrix HfO_2 as compared with the lower-dielectric constant AlN matrix.

Index Terms: Light-material interactions, quantum dots, nanostructures, nonlinear optical effects in semiconductors.

1. Introduction

The study of the optical properties of semiconductor quantum dot (QD) embedded in different dielectrics has gained much attention in recent past due to its novel applications in the field of light emitting devices [1], floating gate memory devices [2], [3], solar cells [4], [5], photovoltaic devices [6] and lasers [7]–[9]. Studies on photo induced intraband transitions and photoelectric processes in QDs are useful in developing QD infrared phototransistors [10]. These applications arises as the manifestation of nanoscale dimension, dielectric confinement, and polarization effects at the interface of QD and the matrix material in which the dot is embedded. The quantum confinement leads to discrete energy levels whereas dielectric mismatch at the dot-matrix interface determines the extent of polarization. The conduction band offset determines the confining barrier height at the dot-matrix interface [11], [12]. Thus, surrounding matrix plays an important role in deciding the optical properties of QDs. The optical properties of QDs can be tailored by changing the dot size

and matrix material. In the interaction of low intensity radiation with matter the induced polarization depends linearly on the electric field of the incident radiation. On increasing the intensity of incident radiation the nonlinear term in the induced polarization becomes important leading to the nonlinear optical behavior. Understanding the linear and the nonlinear optical properties of the QDs effected by their surrounding medium are of immense importance for the realization of ultrafast and efficient optoelectronic devices [1]–[7], [9], [13], [14]. Studies on the optical properties of the QD embedded in matrices of high-dielectric constant [2], [3] and III-N matrix [15], [16] are of particular interest due to their various device applications [2], [3], [17].

In the literature several studies are reported on ZnO QDs embedded in different matrices [1], [4], [14], [18], [19]. Although, AlN matrix [15]–[17], [20] and high-dielectric constant oxide matrix [2], [3] HfO_2 are used for embedding Ge [2], [15], GaN [16], [17], [20] QDs, and Au $-$ Al_2O_3 core-shell [3] QDs, but, ZnO QDs embedded in AlN and HfO_2 matrix are not as such reported. Some reports are available on the fabrication of nanocrystalline ZnO embedded Zr-doped HfO_2 high-k dielectric [21] and on the fabrication of AlN/ZnO coaxial nanotube heterostructures [22]. We expect the synthesis of ZnO QDs in HfO_2 and AlN matrix in future.

We consider QD of ZnO embedded in the high-dielectric oxide (HfO_2, $\varepsilon_r = 25$) and the nitride (AlN, $\varepsilon_r = 8.5$) matrices. The choice of high-dielectric HfO_2 as a matrix material for ZnO QDs would be useful due to its thermal and kinetic stability, low synthesis temperature and sufficient conduction band offset at the interface to act as barrier for electrons [12], [23], [24]. Moreover, due to the high-dielectric constant HfO_2 would minimize the leakage current in devices and maintain high capacitance [23]. ZnO QD embedded in HfO_2 matrix provides the conduction band offset of 2.2 eV at the dot-matrix interface [12]. For matrix with high-dielectric constant the local field factor get strongly enhanced as well as the induced self polarization energy due to charging of the dot changes the confinement potential and consequently affects the optical properties of QD.

The QDs embedded in III-N materials has also a considerable potential for realization of intersublevel (ISL) devices such as quantum dot IR photodetectors [17]. To the best of our knowledge, so far no studies on the ISL linear and nonlinear optical properties are reported on ZnO QDs surrounded by AlN matrix. To explore the effect of III-N confinement on the optical properties, we choose ZnO QD embedded in III-N (AlN) matrix. Due to high epitaxial compatibility of such heterostructure, strain effects get reduced to a good extent with lattice mismatches [11] between 4%–9%. Also, in ZnO/AlN there is a possibility of ISL transitions in near infrared spectral range as a direct consequence of strong carrier localization due to a large conduction band offset [11] 3.29 eV.

In the interaction of optical near field with nanostructures the quadrupole effects plays an important role in modifying the optical absorption spectra [25 and references therein]. The consideration of electric quadrupole effects along with electric dipole effects uncovers transitions which are usually dipole forbidden [26]. In the dipole approximation the incident photon frequency satisfies condition $\vec{k}_{ph} \cdot \vec{r} \ll 1$ condition. $\vec{k}_{ph}$ is the incident photon wave vector and $\vec{r}$ is the electron coordinate in the dot. In electronic transitions the electric quadrupole contribution to transition matrix element corresponds to the term linear in $\vec{k}_{ph} \cdot \vec{r}$ in the expansion of photon plane wave $e^{i\vec{k}_{ph} \cdot \vec{r}}$, whereas replacing it by unity gives the dipole approximation [27]. So far no studies are reported on ZnO/HfO_2 and ZnO/AlN QDs with the inclusion of the quadrupole effects. The present study with the dipole and the quadrupole allowed transitions in ZnO/HfO_2 and ZnO/AlN would be a useful guide to experimental studies.

In 1990 Kayanuma and Momiji introduced a finite square well effective mass approximation [28] (EMA). Several studies based on EMA with finite barrier height [28]–[34] are reported in the literature on embedded QDs. It is reported that for a wide band gap material like ZnO the use of EMA with finite confining potential is suitable as the EMA has been found to predict satisfactorily the energy of the quantum confined states in the ZnO dot [25], [35].

In the present work, we study the optical ISL transitions in the conduction band of a singly charged ZnO QD in the framework of the dipole plus quadrupole approximation. In most of the earlier works on optical transitions in dots only the dipole approximation has been used. We use the EMA with finite barrier height to investigate the linear and the nonlinear optical absorption coefficient for the ZnO QD embedded in AlN and HfO_2 matrix. We also investigate the photoelectric

process in which the electron ejects out from the conduction band. We estimate the dipole and the quadrupole contributions to the photoelectric cross section for both surrounding matrices. It is also important to mention that the impurities and defect states at the dot-matrix interface act as charge trap centers (states) for electrons which can be possibly minimized by passivation [36], [37]. Experimentally, such defects can also be reduced to a good extent by monitoring synthesis conditions [37]. In our present study we consider the dot—matrix interface free from defect states.

2. Theory

Within the framework of the EMA the wave functions of an electron confined in an embedded QD are obtained by solving the Schrödinger equation,

$$\left[-\frac{\hbar^2\nabla^2}{2m^*} + V_{conf}(\vec{r}) + \Sigma(\vec{r})\right]\psi(\vec{r}) = E\psi(\vec{r}) \tag{1}$$

where m^* is the effective mass of the electron in the QD, $V_{conf}(\vec{r})$ is the confinement potential due to the conduction band offset, and $\Sigma(\vec{r})$ is the self energy. The confinement potential is given by,

$$V_{conf}(r) = \begin{cases} 0 & r < R \\ V_b & r \geq R \end{cases} \tag{2}$$

where R is the dot radius and V_b is the finite barrier height. An electron confined in a nanostructure of the dielectric constant ε_{in} surrounded by a matrix of the dielectric constant ε_{out} experiences a dielectric force. The self energy $\Sigma(\vec{r})$ of the electron due to the interaction between the electron and the induced charges at the interface due to the polarization of the dielectric is given by [38],

$$\Sigma(r) = \frac{e^2}{8\pi\varepsilon_0 R}\sum_{n=0}^{\infty}\frac{(\varepsilon_{in}-\varepsilon_{out})(n+1)}{\varepsilon_{in}[\varepsilon_{out}+n(\varepsilon_{in}+\varepsilon_{out})]}\left(\frac{r}{R}\right)^{2n}. \tag{3}$$

The above equation can be expressed as,

$$\Sigma(r) = \frac{1}{2}\left(\frac{1}{\varepsilon_{out}} - \frac{1}{\varepsilon_{in}}\right)\frac{e^2}{4\pi\varepsilon_0 R} + \delta\Sigma$$

with

$$\delta\Sigma = \frac{e^2}{8\pi\varepsilon_0 R}\left(\frac{\varepsilon_{in}-\varepsilon_{out}}{\varepsilon_{in}(\varepsilon_{in}+\varepsilon_{out})}\right)J(\eta, x)$$

where

$$J(\eta, x) = \sum_{n=1}^{\infty}\frac{(n+1)}{(n+\eta)}x^n, x = \frac{r^2}{R^2}, \eta = \frac{\varepsilon_{out}}{(\varepsilon_{in}+\varepsilon_{out})}.$$

When averaged over the probability distribution of the electron, confined strongly in a spherical quantum dot, $\delta\Sigma$ can be approximated as [38]–[40], for $(\varepsilon_{in}+\varepsilon_{out}) \gg 1$,

$$\delta\Sigma \cong 0.47\frac{e^2}{4\pi\varepsilon_0\varepsilon_{in}R}\left(\frac{\varepsilon_{in-}\varepsilon_{out}}{\varepsilon_{in+}\varepsilon_{out}}\right) \tag{4}$$

where e is the electronic charge and ε_0 is the permittivity of free space. The wave functions of the electron in the inner and outer regions of the dot are [41],

$$\psi_{n\ell m}(r,\theta,\phi) = X_{n\ell}(r)Y_{\ell m}(\theta,\phi)$$

TABLE 1

Materials parameters used in the calculation

Materials	V_b (eV) with ZnO	ε_r	m*
HfO_2	2.2 (Ref. 12)	25 (Ref. 24)	$0.11m_e$ (Ref. 45-46)
AlN	3.2 (Ref. 11)	8.5 (Ref. 43)	$0.32m_e$ (Ref. 43-44)
ZnO	-	8.66 (Ref. 25)	$0.24m_e$ (Ref. 41)

where X is the radial function and Y is the spherical harmonic.

$$X_{n\ell}(r) = A_\ell j_\ell(\alpha r), \text{for } r < R$$
$$X_{n\ell}(r) = B_\ell h_\ell(i\beta r), \text{for } r \geq R \tag{5}$$

j_ℓ is the spherical Bessel function, and h_ℓ is the spherical Hankel function. A_ℓ and B_ℓ are the normalization constants. The Ben Daniel - Duke boundary condition [42] at the interface of the dot and the matrix material leads to a transcendental equation,

$$m^*_{out}\alpha h_\ell(i\beta r)[\ell j_{\ell-1}(\alpha R) - (\ell+1)j_{\ell+1}(\alpha R)] = im^*_{in}\beta j_\ell(\alpha R)[\ell h_{\ell-1}(i\beta r) - (\ell+1)h_{\ell+1}(i\beta r)] \tag{6}$$

with

$$\alpha = \sqrt{\frac{2m^*_{in}(E_{n\ell} - \Sigma)}{\hbar^2}} \quad \beta = \sqrt{\frac{2m^*_{out}(V_b + \Sigma - E_{n\ell})}{\hbar^2}} \tag{7}$$

m^*_{in} and m^*_{out} are the effective masses of the electron in the QD and in the matrix material, respectively. The energy levels $(E_{n\ell})$ are obtained by numerically solving the Equation (6). The different materials parameters used in the calculation are given in the Table 1.

2.1. Absorption Coefficients

The linear and the nonlinear absorption coefficient from the initial state (i) of the electron in the conduction band of the dot is given by [25],

$$\alpha^1(\omega) = \omega\sqrt{\frac{\mu}{\varepsilon_r\varepsilon_0}}\frac{|Z_{if}|^2 e^2\rho\hbar\Gamma_{fi}}{\left[(E_f - E_i - \hbar\omega)^2 + (\hbar\Gamma_{fi})^2\right]} \tag{8a}$$

$$\alpha^{(3)}(\omega, I) = -\omega\sqrt{\frac{\mu}{\varepsilon_r\varepsilon_0}}\frac{1}{n_r\varepsilon_0 c}\sum_f \frac{2I|Z_{if}|^4 e^4\rho\hbar\Gamma_{fi}}{\left[(E_f - E_i - \hbar\omega)^2 + (\hbar\Gamma_{fi})^2\right]^2}$$
$$\times\left\{1 - \frac{|Z_{ff} - Z_{ii}|^2}{4|Z_{fi}|^2} \times \frac{(E_f - E_i - \hbar\omega)^2 - (\hbar\Gamma_{fi})^2 + 2(E_f - E_i)(E_f - E_i - \hbar\omega)}{(E_f - E_i)^2 + (\hbar\Gamma_{fi})^2}\right\}. \tag{8b}$$

The incident photon energy is $\hbar\omega$, ε_r is the real part of relative permittivity, μ is the permeability and ρ is the electron density in quantum dot, $n_r = \sqrt{\varepsilon_r}$ is the refractive index of the semiconductor QD. E_f and E_i are the energies of the confined state of the electron in the QD. I is the intensity and $\hbar\Gamma_{fi}$ the line width (we take $\hbar\Gamma_{fi} = 10$ meV). The transition matrix Z_{if} is given by,

$$Z_{if} = F\langle f|H'|i\rangle \tag{9}$$

F is the local field factor [38] which relates the electric field inside (E_{in}) the QD to the electric field outside (E_{out}) the QD by $E_{in} = FE_{out}$ and is given by,

$$F = \frac{3\varepsilon_{out}}{\varepsilon_{in}+2\varepsilon_{out}}. \tag{10}$$

The interaction of the electromagnetic field with the electron in the conduction band of the QD is given by,

$$H' = (\hat{\varepsilon}\cdot\vec{r}).(e^{i\vec{k}_{ph}\cdot\vec{r}}) \tag{11}$$

where $\hat{\varepsilon}$ is the unit polarization vector and $\vec{k}_{ph}$ is the photon propagation vector. In the electric dipole approximation,

$$\begin{aligned} e^{i\vec{k}_{ph}\cdot\vec{r}} &\approx 1 \\ H' &= D \end{aligned} \tag{12}$$

with $D = \hat{\varepsilon}\cdot\vec{r}$.

In the electric dipole plus quadrupole approximation,

$$H' = D + Q \tag{13}$$

with, $Q = (\hat{\varepsilon}\cdot\vec{r})(i\vec{k}_{ph}\cdot\vec{r})$, For the linear and the circular polarization of the incident radiation,

$$D_L = \sqrt{\frac{4\pi}{3}} r Y_{10}(\hat{r}) \tag{14}$$

$$D_C = -\sqrt{\frac{4\pi}{3}} r Y_{11}(\hat{r}) \tag{15}$$

$$Q_L = \sqrt{\frac{\pi}{30}} ik_{ph} r^2 [(Y_{21}(\hat{r}) - Y_{2-1}(\hat{r}))] \tag{16}$$

$$Q_C = -\sqrt{\frac{\pi}{15}} ik_{ph} r^2 Y_{21}(\hat{r}). \tag{17}$$

2.2. Photoelectric Cross Section

The photoelectric process is described by

$$h\nu + D_i^- \longrightarrow D + e^-$$

D represent a neutral QD and D_i^- a charged QD in the initial state i.

The differential cross section for the photoelectric process in the electric dipole plus quadrupole approximation is given by [48],

$$\frac{d\sigma}{d\Omega_{k_f}} = F^2 \frac{4\pi m^* \alpha_{fs} \omega k_f}{\hbar n_r} |\langle \psi_{k_f} | H' | \psi_i \rangle|^2 \tag{18}$$

where α_{fs} is the fine structure constant. $\vec{k}_f$ is the wave vector of the ejected electron

$$k_f^2 = \frac{2m^*}{\hbar^2}[\hbar\omega - W]. \tag{19}$$

The ionization energy $W = \chi - E_i$, χ is the electron affinity [49]. ψ_i and ψ_{k_f} are wave functions of the bound and the ejected electron, respectively. By taking into consideration the neutrality of the dot on

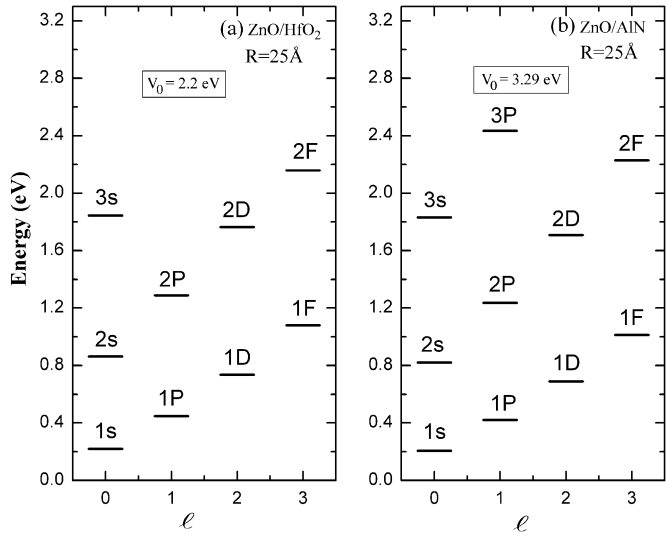

Fig. 1. The confined energy levels $nS(n, \ell = 0)$, $nP(n, \ell = 1)$, $nD(n, \ell = 2)$, and $nF(n, \ell = 3)$ at dot radius R = 25 Å for (a) ZnO/HfO_2; (b) ZnO/AlN.

its ionization we take the ejected electron wave function as a delta function normalized plane wave given by [48],

$$\psi_{k_f}(\vec{r}) = \frac{1}{(2\pi)^{3/2}} e_f^{i\vec{k}_f \cdot \vec{r}}. \tag{20}$$

The total photoelectric cross section is,

$$\sigma_T = \int \frac{d\sigma}{d\Omega_{k_f}} \sin\theta_f d\theta_f d\phi_f = \sigma_D + \sigma_Q. \tag{21}$$

The dipole σ_D and quadrupole σ_Q contributions to the total photoelectric cross section from an initial 1S state of electron in the conduction band of the QD for either state of polarization are obtained as

$$\sigma_D = \frac{8}{3} \frac{F^2 m^*}{\hbar n_r} \pi \omega \alpha_{fs} k_f D_{01}^2 \tag{22}$$

$$\sigma_Q = \frac{2}{15} \frac{F^2 m^*}{\hbar n_r} \pi \omega \alpha_{fs} k_f Q_{02}^2 k_{ph}^2 \tag{23}$$

where,

$$D_{01} = \int_0^R A_0 j_0(\alpha r) r^3 j_1(k_f r)\, dr + \int_R^\infty B_0 h_0(i\beta r) r^3 j_1(k_f r)\, dr \tag{24}$$

$$Q_{02} = \int_0^R A_0 j_0(\alpha r) r^4 j_2(k_f r)\, dr + \int_R^\infty B_0 h_0(i\beta r) r^4 j_2(k_f r)\, dr. \tag{25}$$

3. Results

Fig. 1(a) and (b) shows the confined discrete energy levels (obtained using Equation (6)) nS, nP, nD, and nF of singly charged ZnO QD of radius 25 Å embedded in HfO_2 and AlN matrices. It is found that the confined energy levels in the dot are different in numbers and energy values for

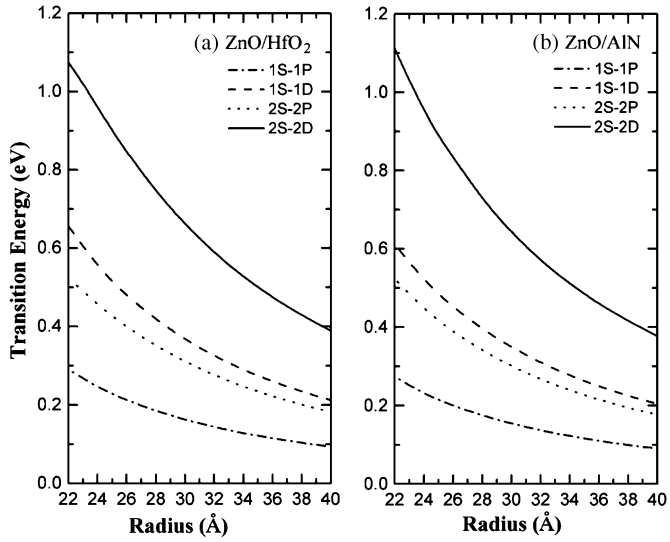

Fig. 2. The variation of transition energy for (1S-1P), (1S-1D), (2S-2P) and (2S-2D) transitions, as a function of dot radius for (a) ZnO/HfO_2; (b) ZnO/AlN.

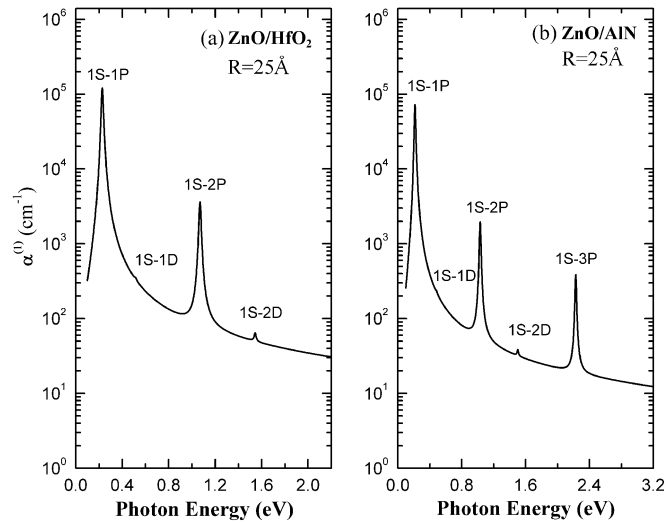

Fig. 3. The variation of the linear absorption coefficient (a) ZnO/HfO_2; (b) ZnO/AlN as a function of photon energy for electron in the initial 1S state in conduction band of the QD of radius R = 25 Å.

different surrounding matrix. In case of the HfO_2 surrounding matrix the energy levels are only up to the 2F level whereas in the AlN matrix the energy levels are up to the 3P level. It is due to the lower conduction band offset (2.2 eV) for ZnO/HfO_2 as compared to the higher conduction band offset (3.29 eV) for ZnO/AlN.

Fig. 2(a) and (b) shows the variation of transition energies with the dot radius for the dipole (1S-1P, 2S-2P) and quadrupole (1S-1D, 2S-2D) ISL transitions for ZnO QD surrounded by HfO_2 and AlN matrices. It is noticed that for an ISL transition, with increasing dot radius transition energy decreases for both the matrices. For an ISL transition the transition energy is relatively higher for the HfO_2 matrix as compared to the AlN matrix.

Fig. 3(a) and (b) shows the variation of the linear absorption coefficient $\alpha^{(1)}$ with the incident photon energy for singly charged ZnO QD from its initial ground state 1S for HfO_2 and AlN matrices at dot radius 25 Å. Absorption peaks corresponding to the dipole and the quadrupole allowed ISL

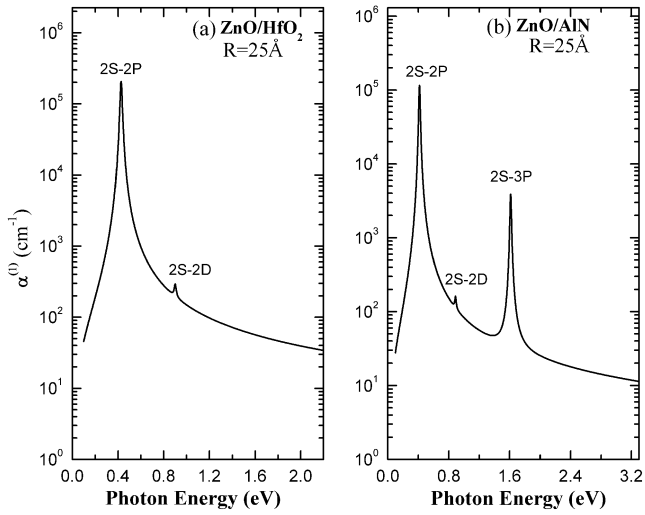

Fig. 4. The variation of the linear absorption coefficient (a) ZnO/HfO_2; (b) ZnO/AlN as a function of photon energy for electron in the initial 2S state in conduction band of the QD of radius R = 25 Å.

transitions in the conduction band are predicted. The number of absorption peaks is restricted by the available confined energy states and their symmetry. The ISL electric dipole transitions are forbidden between confined states with the same symmetry. For HfO_2 matrix, the transition peak positions corresponding to (1S-1P), (1S-1D), (1S-2P) and (1S-2D) transitions are found at incident photon energy values 0.23 eV, 0.52 eV, 1.07 eV and 1.54 eV, respectively. For the AlN matrix the transition peak positions corresponding to (1S-1P), (1S-1D), (1S-2P), (1S-2D) and (1S-3P) transitions are found at energy values 0.21 eV, 0.48 eV, 1.03 eV, 1.50 eV and 2.23 eV. The absorption peak heights corresponding to the dipole $(\Delta\ell = \pm 1)$ transitions are relatively higher as compared to the quadrupole $(\Delta\ell = \pm 2)$ transitions because of the higher values of the transition matrix for dipole allowed transitions. The magnitude of linear absorption coefficient $\alpha^{(1)}$ for the HfO_2 matrix at peak positions is larger compared to the AlN matrix. It is mainly due to the high-dielectric constant of HfO_2 which strongly enhances the local field effect. The local field factor F for the HfO_2 and the AlN surroundings are 1.279 and 0.993, respectively. The absorption coefficient has a square dependence on the F (Equations (8a) and (9)). The self polarization energy induced due to the charging of the QD also influences the energy eigenstates of the QD and the absorption coefficient. In the case of the AlN surrounding matrix the value of self energy is positive whereas in the case of the HfO_2 matrix it is negative. For a fixed dot radius the absorption coefficients for both the dipole and quadrupole transitions are obtained relatively higher for HfO_2 surrounding as compared to AlN surrounding. The peak position of absorption coefficient for transitions from the ground state shifts towards higher energy value for the HfO_2 matrix as compared to AlN matrix due to the relatively higher transition energies in the case of the ZnO/HfO_2.

Fig. 4(a) and (b) shows the variation of the linear absorption coefficient $\alpha^{(1)}$ for the ZnO QD of radius 25 Å for the dipole and quadrupole allowed transitions from its initial excited 2S state in the conduction band for the HfO_2 and AlN surrounding matrices. For the HfO_2 matrix the peak positions corresponding to (2S-2P) and (2S-2D) transitions are found at incident photon of energy values 0.43 eV and 0.90 eV, respectively. For the AlN matrix the peak positions of (2S-2P), (2S-2D) and (2S-3P) transitions are found at 0.42 eV, 0.89 eV, and 1.61 eV incident photon energies, respectively. Similar to the absorption from the ground state (1S) (Fig. 3), also for the absorption from the initial excited state (2S), the absorption peak heights of the dipole $(\Delta\ell = \pm 1)$ transitions are found to be higher compared to the quadrupole $(\Delta\ell = \pm 2)$ transitions. It is found that for a particular transition the magnitude of linear absorption coefficient $\alpha^{(1)}$ for HfO_2 matrix is relatively higher as compared to AlN matrix. It is also noticed that the peaks corresponding to the quadrupole $(\Delta\ell = \pm 2)$ allowed

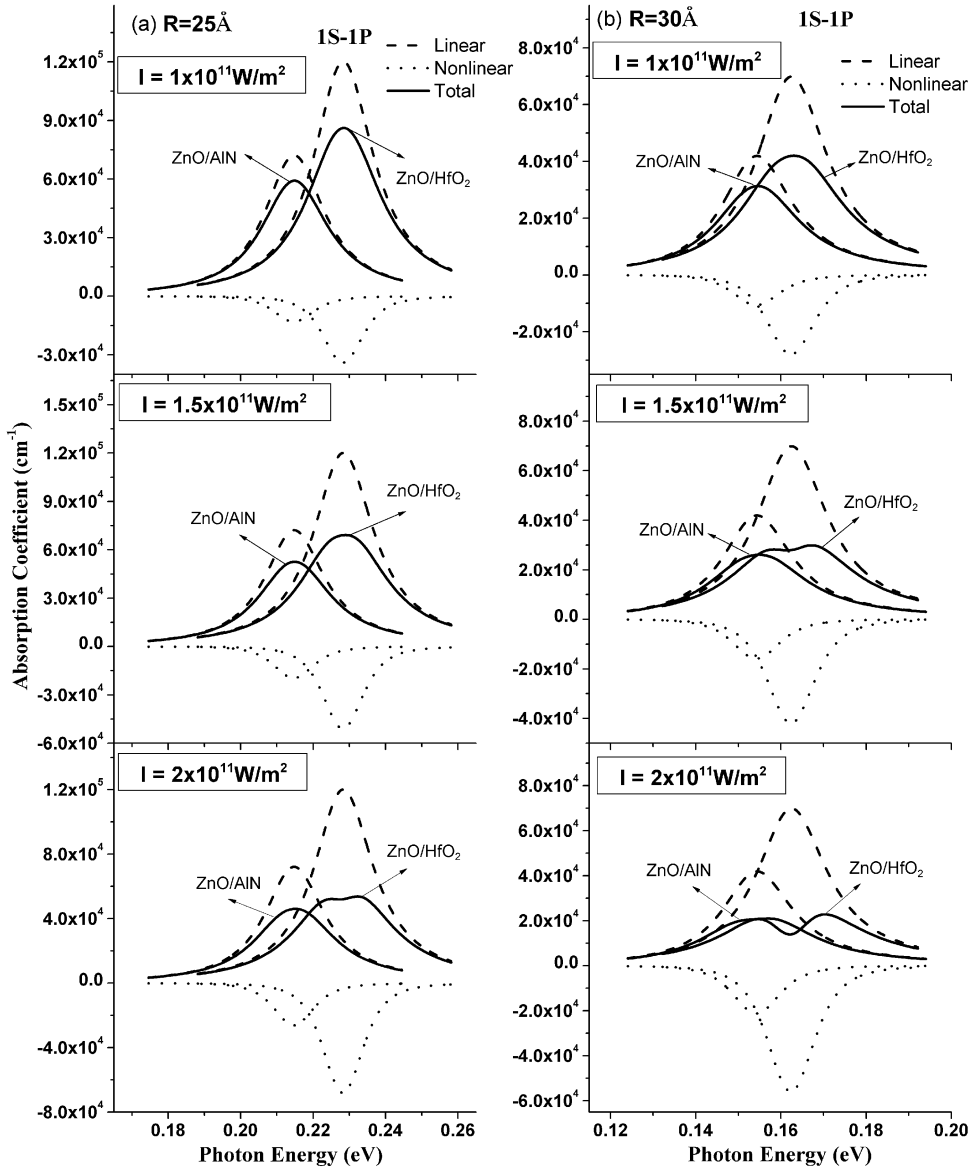

Fig. 5. The variation of the total photoabsorption coefficient for (1S-1P) transition for (a) R = 25 Å; (b) R = 30Å at intensities I = 1.0 × 10^{11}W/m^2; I = 1.5 × 10^{11}W/m^2; and I = 2 × 10^{11}W/m^2 for ZnO/HfO_2 and ZnO/AlN as a function of the incident photon energy,. . . . . ., nonlinear, ___, linear, ____, total.

transitions from the excited 2S state are relatively more pronounced as compared to the quadrupole allowed transitions from the 1S state for both surrounding matrices. This is due to the higher value of transition energies and the transition matrix element for the transitions from the initial 2S state as compared to the transitions from the initial 1S state.

Fig. 5(a) and (b) shows the variation with energy of the linear, the nonlinear, and the total photoabsorption coefficient for QD radius (a) R = 25 Å; and (b) R = 30 Å at three intensities of incident radiation viz: I = 1 × 10^{11} W/m^2; I = 1.5 × 10^{11} W/m^2; and I = 2 × 10^{11} W/m^2 for ZnO QD embedded in HfO_2 and AlN matrix. It is found that the total photoabsorption coefficient is maximum for HfO_2 surrounding due to its high dielectric constant. The high dielectric constant causes negative self polarization contribution to the confinement potential. Also, it leads to higher local field factor for HfO_2 matrix. The local field factor for the ZnO dot in HfO_2 and AlN matrices are 1.279 and 0.993, respectively. Hence, due to competitive combined effect of local field factor and confinement

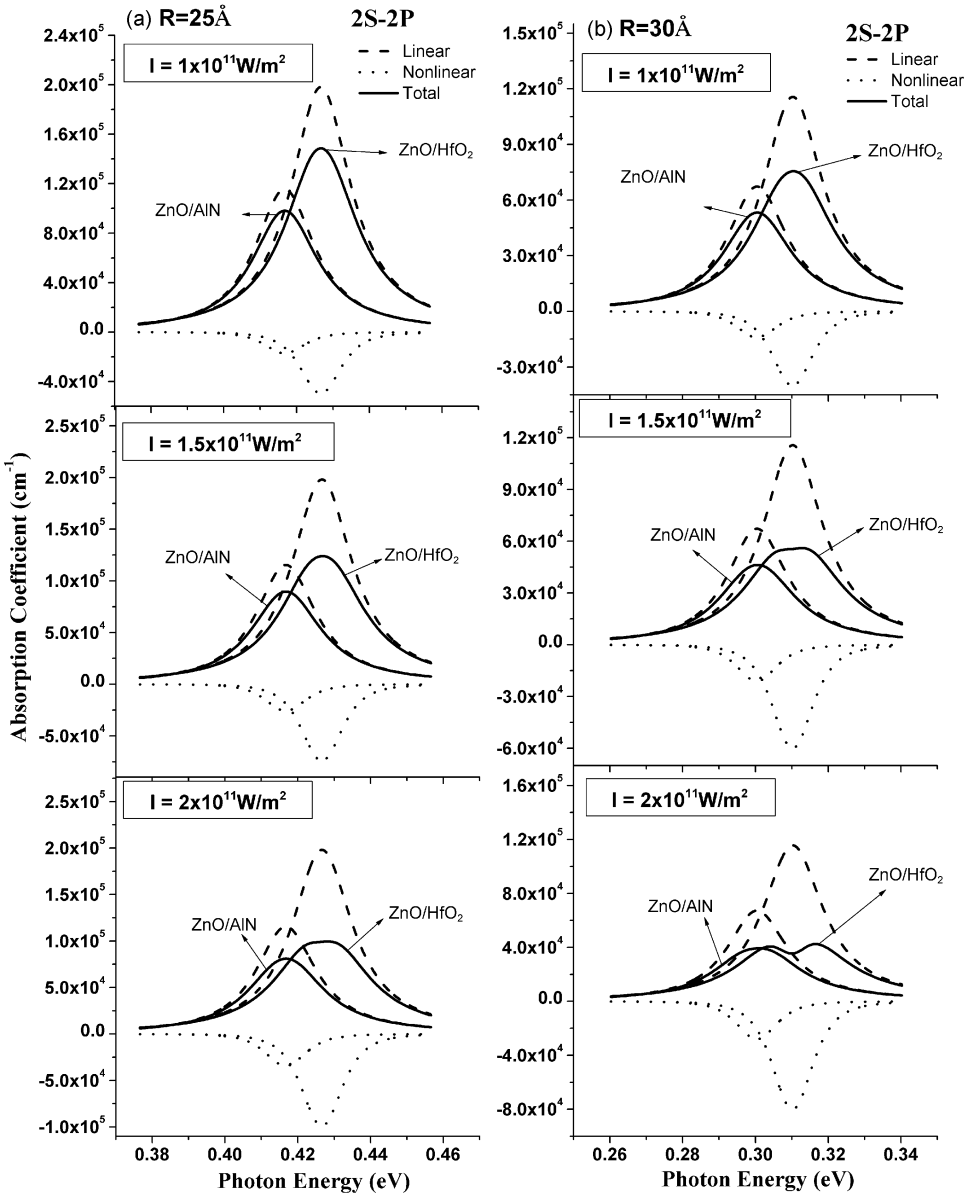

Fig. 6. The variation of the total photoabsorption coefficient for (2S - 2P) transition for (a) R = 25 Å; (b) R = 30 Å at intensities I = 1 × 10^{11} W/m^2; I = 1.5 × 10^{11}W/m^2; and I = 2 × 10^{11} W/m^2 for ZnO/HfO_2 and ZnO/AlN as a function of the incident photon energy, ..., nonlinear, ___, linear, ____, total.

potential the HfO_2 matrix leads to higher total ISL absorption coefficient in comparison to AlN matrix. From Fig. 5(a) and (b) we also find that QD size and the confinement potential influence the total ISL absorption coefficient. The total photoabsorption coefficient for a surrounding matrix decreases with increasing dot size due to its inverse dependence on the QD volume. For both the surrounding matrices, on increasing the intensity at a fixed dot radius, the relative difference between peak heights of the total absorption in the AlN and HfO_2 surrounding matrices decreases with increase in intensity. This is due to a relatively larger nonlinear negative contribution to the total photo-absorption for the high-dielectric HfO_2 surrounding matrix compared to the AlN surrounding. For HfO_2 bleaching is obtained at higher intensity where the total absorption coefficient peak splits into two peaks because of the large negative nonlinear contribution. On increasing the intensity of incident radiation bleaching effect is pronounced in the HfO_2 matrix as compared to the AlN matrix.

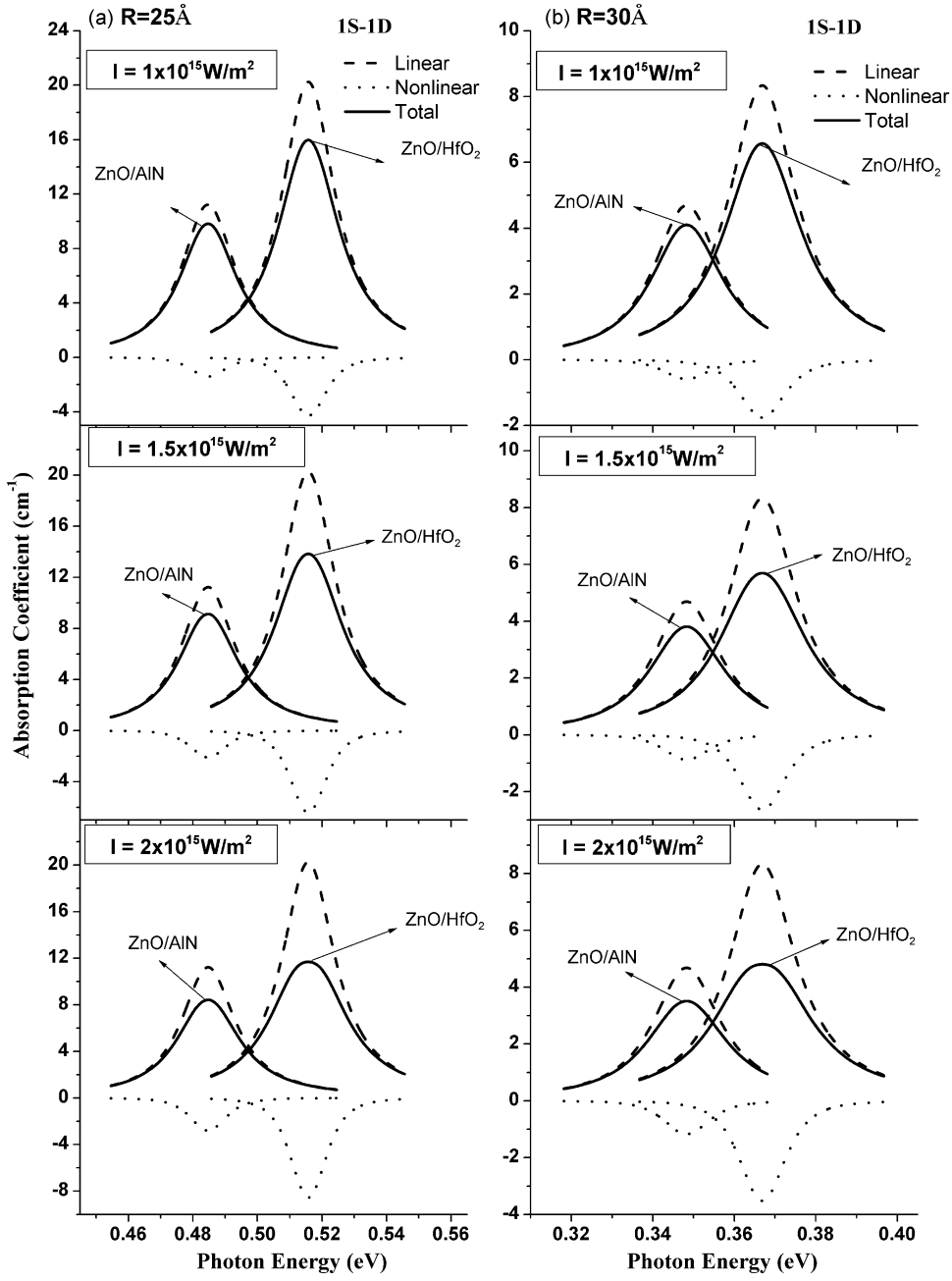

Fig. 7. The variation of the total photoabsorption coefficient for (1S-1D) transition for (a) R = 25 Å; (b) R = 30 Å at intensities I = 1 × 10^{15} W/m^2; I = 1.5 × 10^{15} W/m^2; and I = 2 × 10^{15} W/m^2 for ZnO/HfO_2 and ZnO/AlN as a function of the incident photon energy ....., nonlinear, ___, linear, ____, total.

For both the matrices HfO_2 and AlN, it is noticed from Fig. 5 (for initial1S state) and Fig. 6 (for initial 2S state) that the magnitude of the photoabsorption peak height for the transition from initial 2S state is relatively higher as compared to the peak height for the transition from initial 1S state. This is because of the higher value of the transition matrix from initial 2S state compared to the transition matrix from initial 1S state.

For the energy range shown in Figs. 5 and 6 the main contribution to absorption coefficient comes from the dipole allowed transitions 1S-1P and 2S-2P, respectively and the quadrupole contribution is negligible.

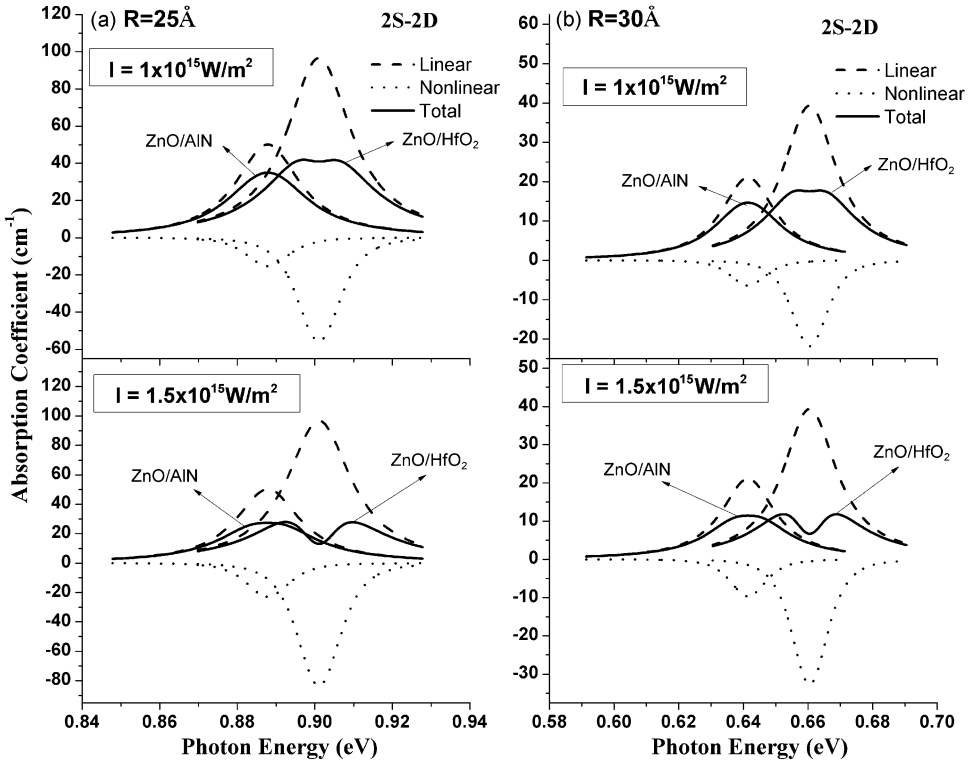

Fig. 8. The variation of the total photoabsorption coefficient for (2S - 2D) transition for (a) R = 25 Å; (b) R = 30 Å at intensities I = 1 × 10^{15} W/m^2; and I = 1.5 × 10^{15} W/m^2 for ZnO/HfO_2 and ZnO/AlN as a function of the incident photon energy. . . . . ., nonlinear, _____, linear, ____, total.

Figs. 7 and 8 shows the variation with energy of absorption coefficient from initial 1S and 2S state, respectively at dot radius (a) R = 25 Å; and (b) R = 30 Å at three intensities of incident radiation viz: I = 1 × 10^{15} W/m^2; I = 1.5 × 10^{15} W/m^2; and I = 2 × 10^{15} W/m^2. It is noticed that in this energy range the main contribution to the absorption comes from the quadrupole transition 1S-1D (Fig. 7) and 2S-2D (Fig. 8). Due to the weak strength of the quadrupole transitions, the nonlinear contributions in quadrupole transitions become noticeable at higher intensities. The bleaching effect is also noticeable at higher intensities (Fig. 8).The magnitudes of the total photoabsorption coefficients in Figs. 7 and 8 are much lower compare to those in Figs. 5 and 6 because of the lower value of quadrupole matrix compared to the dipole matrix. Further, similar to the dipole ISL transitions the total photoabsorption coefficient for the quadrupole ISL transitions will also decrease on increasing the dot size due to inverse dependence on the dot volume.

The surrounding matrix material of high dielectric constant [12] provides a large dielectric discontinuity at the dot-matrix interface. Such material would be suitable for observing a prominent quadrupole effect on the photoabsorption [26]. A large dielectric discontinuity causing a large local electric field gradient [50] would account for strong quadrupole transition strength.

Fig. 9(a) and (b) shows the variation of the photoelectric cross section with incident photon energy from the initial 1s state of the ZnO quantum dot embedded in AlN and HfO_2 matrices. Two dot radii R = 20 Å and R = 25 Å are considered. For both the surrounding matrices, it is found that the contribution of the dipole and the quadrupole photoelectric cross sections to the total photoelectric cross section decreases on increasing the incident photon energy. This is due to decrease in the value of photoelectric transition matrix (Equation (18)) with increase in incident photon energy. Also, we note that for energies greater than threshold the dipole and the quadrupole contribution to the photoelectric cross section for the dot radius 25 Å are lower compared to the cross sections at dot radius 20 Å for both the matrices. This is because the photoelectric cross section depends on the wave vector of ejected electron and the overlap of the initial state wave

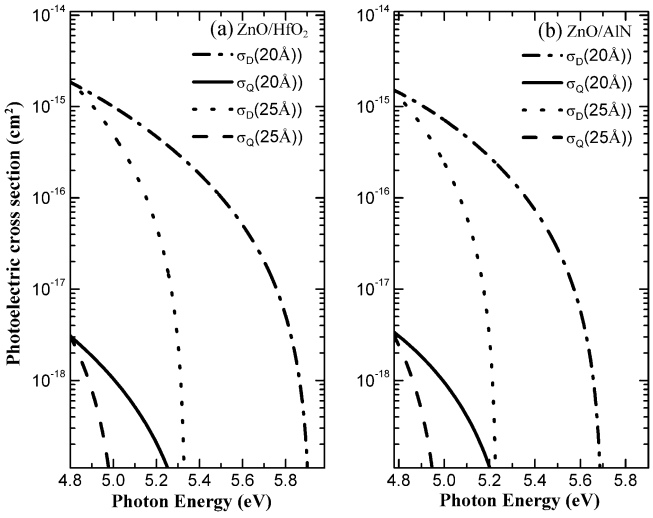

Fig. 9. The variation of photoelectric cross section with incident photon energy from the initial 1S state of the QD of radius R = 20 Å; and R = 25 Å for (a) ZnO/HfO_2 and (b) ZnO/AlN _._._._, σ_D for R = 20 Å, ____, σ_Q for R = 20 Å, ... , σ_D for R = 25 Å, _ _ _ _, σ_Q for R = 25 Å.

function and the ejected electron wave function in the photoelectric transition matrix (Equation (18)). With the increase in the dot radius the wave function and energy of the state 1S change and lead to the lowering of the cross section. The contribution of the dipole cross section to the total photoelectric cross section at a given radius is relatively higher for the HfO_2 matrix as compared to the AlN matrix while the quadrupole cross section contribution to the total photoelectric cross section at a given radius is found to be nearly equal for both the matrices.

4. Conclusion

The inclusion of electric quadrupole effect modifies the absorption spectra of singly charged ZnO QD embedded in dielectric matrix. In the absorption spectra of the QD, peaks corresponding to quadrupole allowed transitions, although weak, appear in addition to the peaks corresponding to the dipole allowed transitions. It is found that the total photoabsorption coefficient and the photoelectric cross section depend significantly on the confinement potential, the surrounding matrix, and the local field. The intensity of incident radiation strongly influences the nonlinear absorption coefficient and at higher intensities bleaching is observed in total photoabsorption coefficient. The photoabsorption coefficients are found to be higher in magnitude for HfO_2 as compared to AlN matrix. The dielectric constant of the surrounding matrix influences the local field, self energy, and confinement potential leading to significant changes in the optical properties of the QD. The HfO_2 matrix could be a better choice in emerging "high-dielectric" based nano-optoelectronic devices. Present study would be a useful guide to develop optoelectronic devices such as QD intersubband infrared photodetectors and phototransistors based on photoabsorption and photoelectric processes in ZnO/HfO_2, and ZnO/AlN QDs.

Acknowledgment

We thank the Jaypee Institute of Information technology, Noida for providing facilities and support to carry out this work.

References

[1] J. H. Lim, K. H. Lee, and D. C. Lim, "ZnO light emitting diode using ZnO quantum dots embedded in an amorphous silicon-oxide matrix," *J. Korean Phys. Soc.*, vol. 58, no. 6, pp. 1664–1667, Jun. 2011.

[2] S. K. Ray, S. Das, R. K. Singha, S. Manna, and A. Dhar, "Structural and optical properties of germanium nanostructures on Si (100) and embedded in high-k oxides," *Nanosc. Res. Lett.*, vol. 6, no. 1, pp. 224-1–224-10, Mar. 2011.
[3] Z. Xu *et al.,* "Improved performance of non-volatile memory with Au-Al_2O_3 core-shell nanocrystals embedded in HfO_2 matrix," *Appl. Phys. Lett.*, vol. 100, no. 20, pp. 203509-1–203509-4, May 2012.
[4] J. Gao *et al.,* "Quantum dot size dependent J-V characteristics in heterojunction ZnO/PbS quantum dot solar cells," *Nano Lett.*, vol. 11, no. 3, pp. 1002–1008, Mar. 2011.
[5] R. Loef, A. J. Houtepen, E. Talgorn, J. Schoonman, and A. Goossens, "Study of electronic defects in CdSe quantum dots and their involvement in quantum dot solar cells," *Nano Lett.*, vol. 9, no. 2, pp. 856–859, Feb. 2009.
[6] S. Mirabella *et al.,* "Matrix role in Ge nanoclusters embedded in Si_3N_4 or SiO_2," *Appl. Phys. Lett.*, vol. 101, no. 1, pp. 011911-1–011911-5, Jul. 2012.
[7] A. Passaseo, G. Maruccio, M. D. Vittorio, R. Rinaldi, and R. Cingolani, "Wavelength control from 1.25 to 1.4 μm in $In_xGa_{1-x}As$ quantum dot structures grown by metal organic chemical vapour deposition," *Appl. Phys. Lett.*, vol. 78, no. 10, pp. 1382–1384, Mar. 2001.
[8] B. A. Ghalib, S. J. Al-Obaidi, and A. H. Al-Khursan, "Quantum dot semiconductor laser with optoelectronic feedback," *Superlattices Microstr.*, vol. 52, no. 5, pp. 977–986, Nov. 2012.
[9] Y. Qiu, P. Gogna, S. Forouhar, A. Stintz, and L. F. Lester, "High-performance InAs quantum-dot lasers near 1.3 μm," *Appl. Phys. Lett.*, vol. 79, no. 22, pp. 3570–3572, Nov. 2001.
[10] V. Ryzhii, "The theory of quantum-dot infrared phototransistors," *Semicond. Sci. Technol.*, vol. 11, no. 5, pp. 759–765, May 1996.
[11] T. D. Veal *et al.,* "Valence band offset of ZnO/AlN heterojunction determined by X-ray photoemission spectroscopy," *Appl. Phys. Lett.*, vol. 93, no. 20, pp. 202108-1–202108-3, Nov. 2008.
[12] J. Robertson and B. Falabretti, "Band offsets of high k gate oxides on III-V semiconductors," *J. Appl. Phys.*, vol. 100, no. 1, pp. 014111-1–014111-8, Jul. 2006.
[13] N. Nuntawong *et al.,* "Quantum dot lasers based on stacked and strain-compensated active region grown by metal-organic chemical vapour deposition," *Appl. Phys. Lett.*, vol. 86, no. 19, pp. 193115-1–193115-3, May 2005.
[14] U. Zope, E. P. Samuel, M. P. Bhole, and D. S. Patil, "Optical field distribution in ZnO/MgZnO quantum dot nanostructure at 375-nm wavelength," *Phys. E*, vol. 42, no. 1, pp. 38–42, Nov. 2009.
[15] K. M. Hassan, A. K. Sharma, J. Narayan, J. F. Muth, C. W. Teng, and R. M. Kolbas, "Optical and structural studies of Ge nanocrystals embedded in AlN matrix fabricated by pulsed laser deposition," *Appl. Phys. Lett.*, vol. 75, no. 9, pp. 1222–1224, Aug. 1999.
[16] J. Renard, R. Songmuang, C. Bougerol, B. Daudin, and B. Gayral, "Exciton and biexciton luminescence from single GaN/AlN quantum dots in nanowires," *Nano Lett.*, vol. 8, no. 7, pp. 2092–2096, Jul. 2008.
[17] A. Vardi *et al.,* "Room temperature demonstration of GaN/AlN quantum dot intraband infrared photodetector at fiber-optics communication wavelength," *Appl. Phys. Lett.*, vol. 88, no. 14, pp. 143101-1–143101-3, Apr. 2006.
[18] Z. Zeng, E. Paspalakis, C. S. Garoufalis, A. F. Terzis, and S. Baskoutas, "Linear and nonlinear optical properties of ZnO/ZnS and ZnS/ZnO core shell quantum dots: Effects of shell thickness, impurity, and dielectric environment," *J. Appl. Phys.*, vol. 114, no. 2, pp. 023510-1–023510-9, Jul. 2013.
[19] Y. Y. Peng, T. E. Hsieh, and C. H. Hsu, "Dielectric confinement effect in ZnO quantum dots embedded in amorphous SiO_2 matrix," *J. Phys. D, Appl. Phys.*, vol. 40, no. 19, pp. 6071–6075, Oct. 2007.
[20] A. Vardi, G. Bahir, S. E. Schacham, P. K. Kandaswamy, and E. Monroy, "Photocurrent spectroscopy of bound-to-bound intraband transitions in GaN/AlN quantum dots," *Phys. Rev. B, Condens. Matter*, vol. 80, no. 15, pp. 155439-1–155439-13, Oct. 2009.
[21] C. H. Lin and Y. Kuo, "Nonvolatile memories with dual-layer nanocrystalline ZnO embedded Zr-doped HfO_2 high-k dielectric," *Electrochem. Solid State Lett.*, vol. 13, no. 3, pp. H83–H86, Dec. 2010.
[22] Y. J. Kim *et al.,* "Position-controlled Aln/ZnO coaxial nanotube heterostructure arrays for electron emitter applications," *Nanotechnology*, vol. 21, no. 5, pp. 055303-1–055303-5, Feb. 2010.
[23] Q. Chen *et al.,* "Band offsets of HfO_2 interface: In situ X-ray photoelectron spectroscopy measurement and ab initio calculation," *Appl. Phys. Lett.*, vol. 95, no. 16, pp. 162104-1–162104-3, Oct. 2009.
[24] J. Robertson, "High dielectric constant oxides," *Eur. Phys. J. Appl. Phys.*, vol. 28, no. 3, pp. 265–291, Dec. 2004.
[25] D. Maikhuri, S. P. Purohit, and K. C. Mathur, "Quadrupole effects in photoabsorption in ZnO quantum dots," *J. Appl. Phys.*, vol. 112, no. 10, pp. 104323-1–104323-9, Nov. 2012.
[26] J. J. Peterson, L. Huang, C. Delerue, G. Allan, and T. D. Krauss, "Uncovering forbidden optical transitions in PbSe nanocrystals," *Nano Lett.*, vol. 7, no. 12, pp. 3827–3831, Dec. 2007.
[27] A. K. Jain and K. C. Mathur, "Multipole interference effect in the photoionization of sodium," *J. Phys. B, At. Mol. Opt. Phys.*, vol. 26, no. 3, pp. 433–444, Feb. 1993.
[28] Y. Kayanuma and H. Momiji, "Incomplete confinement of electrons and holes in microcrystals," *Phys. Rev. B., Condens. Matter*, vol. 41, no. 14, pp. 10 261–10 263, May 1990.
[29] K. K. Nanda, F. E. Kruis, and H. Fissan, "Energy levels in embedded semiconductor nanoparticles and nanowires," *Nano Lett.*, vol. 1, no. 11, pp. 605–611, Nov. 2001.
[30] K. K. Nanda, F. E. Kruis, H. Fissan, and S. N. Behera, "Effective mass approximation for two extreme semiconductors: Band gap of PbS and CuBr nanoparticles," *J. Appl. Phys.*, vol. 95, no. 9, pp. 5035–5041, May 2004.
[31] G. Pellegrini, G. Mattei, and P. Mazzoldi, "Finite depth square well model: Applicability and limitations," *J. Appl. Phys.*, vol. 97, no. 7, pp. 073706-1–073706-8, Apr. 2005.
[32] S. Baskoutas and A. F. Terzis, "Size dependent exciton energy of various technologically important colloidal quantum dots," *Mater. Sci. Eng. B*, vol. 147, no. 2/3, pp. 280–283, Feb. 2008.
[33] W. Sheng, "Polarization of intersubband transitions in self assembled quantum dots," *Appl. Phys. Lett.*, vol. 92, no. 4, pp. 043113-1–043113-3, Jan. 2008.
[34] J. L. Marin, R. Riera, and S. A. Cruz, "Confinement of excitons in spherical quantum dots," *J. Phys., Condens. Matter.*, vol. 10, no. 6, pp. 1349–1361, Feb. 1998.

[35] A. Germeau *et al.,* "Optical transitions in artificial few-electron atoms strongly confined inside ZnO nanocrystals," *Phys. Rev. Lett.*, vol. 90, no. 9, pp. 097401-1–097401-4, Mar. 2003.
[36] J. J. Siddiqui, Ph.D. dissertation, Univ. Michigan, Ann Arbor, MI, USA, 2012.
[37] S. Parola, E. Quesnel, V. Muffato, J. Bartringer, and A. Slaoui, "Influence of the embedding matrix on optical properties of Ge nanocrystals-based nanocomposite," *J. Appl. Phys.*, vol. 113, pp. 053512-1–053512-8, Feb. 2013.
[38] C. Delerue and M. Lannoo, *Nanostructures: Theory and Modelling*. Berlin, Germany: Springer-Verlag, 2004.
[39] M. Lannoo, C. Delerue, and G. Allan, "Screening in semiconductor nanocrystallites and its consequences for porous silicon," *Phys. Rev. Lett.*, vol. 74, no. 17, pp. 3415–3418, Apr.1995.
[40] P. G. Bolcatto and C. R. Proetto, "Shape and dielectric mismatch effects in semiconductor quantum dots," *Phys. Rev. B., Condens. Matter*, vol. 59, pp. 12 487–12 498, May 1999.
[41] L. E. Brus, "A simple model for the ionization potential, electron affinity, and aqueous redox potentials of small semiconductor crystallites," *J. Chem. Phys.*, vol. 79, no. 11, pp. 5566–5571, Dec. 1983.
[42] G. T. Einevoll and L. J. Sham, "Boundary conditions for envelope functions at interfaces between dissimilar materials," *Phys. Rev. B., Condens. Matter*, vol. 49, no. 15, pp. 10 533–10 542, Apr. 1994.
[43] J. Wu, "When group-III nitrides go infrared: New properties and perspectives," *J. Appl. Phys.*, vol. 106, no. 1, pp. 011101-1–011101-23, Jul. 2009.
[44] P. Rinke *et al.,* "Consistent set of band parameters for the group-III nitrides AlN, GaN, and InN," *Phys. Rev. B., Condens. Matter*, vol. 77, no. 7, pp. 075202-1–075202-15, Feb. 2008.
[45] S. Monaghan, P. K. Hurley, K. Cherkaoui, M. A. Negara, and A. Schenk, "Determination of electron effective mass and electron affinity in HfO_2 using MOS and MOSFET structures," *Solid State Electron.*, vol. 53, no. 4, pp. 438–444, Apr. 2009.
[46] W. J. Zhu, T. P. Ma, T. Tamagawa, J. Kim, and Y. Di, "Current transport in metal/hafnium oxide/silicon structure," *IEEE Electron Device Lett.*, vol. 23, no. 2, pp. 97–99, Feb. 2002.
[47] D. Maikhuri, S. P. Purohit, and K. C. Mathur, "Linear and nonlinear intraband optical properties of ZnO quantum dots embedded in SiO2 matrix," *AIP Adv.*, vol. 2, no. 1, pp. 012160-1–012160-15, Mar. 2012.
[48] S. P. Purohit and K. C. Mathur, "Study of photoabsorption and photoelectric process in GaAs semiconductor quantum dot nanostructure," *J. Comput. Theor. Nanosci.*, vol. 7, no. 6, pp. 1131–1135, Jun. 2010.
[49] J. H. Han, N. Yoshimizu, C. Jiang, A. Lal, and C. H. Lee, "Electroluminescence from a suspended tip-synthesized nano ZnO dot," *Appl. Phys. Lett.*, vol. 9812, pp. 121113-1–112113-3, Mar. 2011.
[50] J. R. Z. Sanchez and L. Novotny, "Multipolar interband absorption in semiconductor quantum dot. I. Electric quadrupole enhancement," *J. Opt. Soc. Amer. B.*, vol. 19, no. 6, pp. 1355–1362, Jun. 2002.